# BHI-Net: Brain-Heart Interaction-Based Deep Architectures for Epileptic Seizures and Firing Location Detection

Nabil Sabor, *Member, IEEE*, Hazem Mohammed, *Student Member, IEEE*, Zhe Li, *Member, IEEE*, and Guoxing Wang, *Senior Member, IEEE*

***Abstract*— Automatic detection of epileptic seizures is still a challenging problem due to the intolerance of EEG. Introducing ECG can help with EEG for detecting seizures. However, the existing methods depended on fusing either the extracted features or the classification results of EEG-only and ECG-only with ignoring the interaction between them, so the detection rate did not improve much. Also, all EEG channels were considered in a complex manner. Moreover, the detection of epilepsy firing location, which is an important issue for diagnosing epilepsy, is not considered before. Therefore, we propose a new method based on the brain-heart interaction (BHI) for detecting the seizure onset and its firing location in the brain with lower complexity and better performance. BHI allows us to study the nonlinear coupling and variation of phase-synchronization between brain regions and heart activity, which are effective for distinguishing seizures. In our method, the EEG channels are mapped into two surrogate channels to reduce the computational complexity. Moreover, the firing location detector is triggered only once the seizure is detected to save the system's power. Evaluation using different proposed classification networks based on the TUSZ, the largest available EEG/ECG dataset with 315 subjects and 7 seizure types, showed that our BHI method improves the sensitivity by 48% with only 4 false alarms/24h compared to using only EEG. Moreover, it outperforms the performance of the average human detector based on the quantitative EEG tools by achieving a sensitivity of 68.2% with 11.9 false alarms/ 24h and a latency of 11.94 sec.**

Manuscript received July 22, 2021; revised January 20, 2022 and April 7, 2022; accepted April 26, 2022. Date of publication June 8, 2022; date of current version June 15, 2022. This work was supported in part by the National Key Research and Development Program of China under Grant 2019YFB2204500 and in part by the National Natural Science Foundation of China under Grant 61874171 and Grant 52077133. *(Corresponding author: Zhe Li.)*

Nabil Sabor is with the Electrical Engineering Department, Faculty of Engineering, Assiut University, Assiut 71516, Egypt (e-mail: nabil_sabor@aun.edu.eg).

Hazem Mohammed and Guoxing Wang are with the Department of Micro-Nano Electronics, Shanghai Jiao Tong University, Shanghai 200240, China, and also with the MoE Key Laboratory of Artificial Intelligence, Shanghai Jiao Tong University, Shanghai 200240, China (e-mail: h.moh.88@aun.edu.eg; guoxing@sjtu.edu.cn).

Zhe Li is with the Academy of Information Technology and Electrical Engineering, Shanghai Jiao Tong University, Shanghai 200240, China (e-mail: zhe_li@sjtu.edu.cn).

Digital Object Identifier 10.1109/TNSRE.2022.3181151

***Index Terms*— Brain-heart Interaction, deep network, EEG, ECG, support vector machine, and wavelet bi-spectrum.**

## I. Introduction

EPILEPSY is the world's most common neurological disease according to the latest data of the World Health Organization (WHO) [1]. Epilepsy originates from recurrent abnormal discharges of the brain's electrical activity, leading to uncontrollable movements and tremulous. Seizures are life-threatening and may cause brain, heart, and/or lung failure and head trauma. It affects people of all ages; however, it is more common in children and people over 65 years. The sudden unexpected death due to epilepsy is the highest compared to the other causes and almost 70 million people around the globe have epilepsy with about two million new cases reported each year [2].

Electroencephalography (EEG) is the key tool for detecting epileptic events because seizure originates from recurrent abnormal discharges of the brain's electrical activity [3]. The diagnosis and treatment of epilepsy depend on detecting the epileptic discharges of the EEG signal and detecting the firing location of these discharges. The manual detection of abnormal epileptic characteristics from EEG is very time-consuming, especially in the case of long-term recordings [4]. Developing automatic systems can help clinicians for detecting epileptic seizures with high precision and also saves the time of neurophysiologists. However, the intolerance and artifacts of EEG recordings are challenges for developing high precision detection systems [5].

Besides the epileptic discharges on the EEG signal, epileptic seizures lead to variations in cardiac autonomic nervous function. These variations and rhythm disturbances happen immediately after the onset of the seizure and may precede the EEG seizure onset in some cases [6]. So, introducing Electrocardiograph (ECG) with EEG for detecting epileptic seizures can overcome the intolerance of EEG and improve the detection rate. The developed work in this area depends on extracting different features from each signal and then fusing the classification results of EEG-only and ECG-only classifiers which increases the system's complexity [7], [8].

TABLE I
STATE-OF-THE-ART METHODS FOR THE DETECTION OF EPILEPTIC SEIZURES

| Ref | Signal | Dataset | Features | Classifier | Post-processing | Performance matrices |
|---|---|---|---|---|---|---|
| [10] | EEG Recordings | **Bonn** (sEEG/iEEG) (Single ch.) 10 subjects, 1 seizure type, 100 seizure occurrence/ 0.6 h, **accessible**. | Shape- and Texture-Based Features | SVM | - | ACC: 98 % |
| [11] | | | Time-domain based features | K-NN | - | ACC: 94.4 % |
| [12] | | | Spectral moment-based features | SVM | - | ACC: 99 % |
| [13] | | | Wavelet coefficients-based features | ANN+ GA | - | ACC: 99.7 % |
| [14] | | | Time and frequency domain features | RF | - | ACC: 98.45 % |
| [15] | | | Time and frequency domain features | BPNN, GA-SVM | - | ACC: > 98.1%, |
| [18] | | | Time-frequency-based using TQWT | RF, K-NN | | SN: 98 %, SP: 97 %, ACC: 99% |
| [20] | | **CHB-MIT** sEEG/23 chs, 22 subjects, 1 seizure type, 198 seizure occurrence/ 2.8h, **accessible**. | Time-domain based features | Thresholding / GA | - | FPR: 0.39/24 h |
| [29] | | | Time domain and Frequency domain features | RF | - | ACC: 99.3%, SP: 83%, SN:99.4%, FAR: 0.57 /h |
| [27] | | | Power-based features using Dynamic Mode Decomposition | Boost decision-tree | Alarm after 10 seizures | SN: 87%, SP: 99%, FAR: 4/24h |
| [21] | | **Freiburg** (iEEG/6 chs.) 21 subjects (8 M/12 F), 1 seizure type, 88 seizures occur., **accessible**. | Time-Frequency domain using WPT | WELM | A moving average filter | SN: 97.73 %, FAR: 0.37/h |
| [22] | | | Time-Frequency domain using DWT | SVM | - | SN: 93 %, SP: 99 % |
| [23] | | | Bi-frequency based features using the Bispectrum method | Two SVM classifiers | OR Fusing and smooth | ACC: 96.8 %, SN: 95.8 %, SP: 96.7 %, FAR: 0~0.8 /h |
| [24] | | **TUSZ** (sEEG/ 22 ch.) 315 subjects, 7 seizure types, 1791 seizures occur. /36 h, **accessible**. | Cepstral-domain and differential energy-based features | CNN/LSTM | Language modeling component | SN: 30.83 %, SP: 96.86 % FAR: 7 / 24 h |
| [25] | | | Discrete Wavelet Transform | CNN | Finite-state-machine | SN: 59 %, SP: 89.72 % FAR: 12 / 24 h |
| [26] | | **Bonn** + **CHB-MIT** (Single ch.) | Kraskov Entropy features of the first three IMFs and the first three sub-bands using TQWT | Least Squares-SVM | - | **Bonn** (ACC:99%, SN:98%, SP:99.5%), **CHB-MIT** (ACC: 69%, SN:74%, SP:64.9%) |
| [28] | | **Bonn** + **CHB-MIT** (Single ch.) | Time-domain +Time-Frequency domain features using HWPT | RVM | - | **CHB-MIT** (ACC:96%, FPR: 0.1 /h, DL:1.89 s), **Bonn** (ACC:99.8%) |
| [31] | ECG Recordings | Recorded (WAG\Rij rats) | Time and frequency-domain features | SVM | - | ACC:73%, SP:76%, SN: 71% |
| [32] | | Physionet dataset (7 subjects) | Temporal and Spectral based features | Threshold approach | 5 min post-ictal | ACC: 94.2 %, SN: 84.1 %, SP: 94.5 % |
| [33] | | 14 subjects/69 seizure 14 subjects/38 seizure | The maximal peak heart rate and the maximal heart rate gradient | Heuristic adaptive | - | SN: 77.6 %, FAR: 2.56 /24 h SN: 96 %, FAR: 1.84 /24 h |
| [8] | ECG and EEG Recordings | **KCH dataset** (sEEG/ 22 chs ECG/ 1 ch.), 12 subjects, 1 seizure type, 633 seizures occur. / 49 h, **not accessible.** | Time and frequency domain features. 6 features for EEG and 6 for ECG. | LDC | Neglecting epochs that have artifacts | ACC: 71.51 %, SN: 71.73 %, SP: 71.43 %, FAR: 28.57% |
| [34] | | | Statistical features based on directions of Gabor function. | K-NN (K=6) | - | **ACC, SN, SP, FAR** **EEG:**84.95,73.1,88.3,11.05 % **EEG-ECG:** 86.1,79.7, 87.79, 11.52% |
| [7] | | **EPILEPSIAE** (sEEG/iEEG, ECG) 24 subjects, 1 seizure type, 183 seizure occurrence, **not free**. | Time-Frequency domain-based features using the Wigner–Ville Distribution and the discrete Wavelet transform | SVM is used separately for ECG and each sub-band of EEG. | **ECG**:3consecutive outputs by 1. **EEG**: OR, AND or MAJ **Final:** AND of ECG and EEG | **AND, OR, MAJ** SN:100, 100, 100 % SP:99.97,99.92,99.95 % FPR: 0.9, 2.5, 1.6 /h DL:17.1, 12,10.8 s |

***SVM:** Support Vector Machine, **K-NN:** K-Nearest Neighbor, **ANN:** Artificial Neural Network, **GA:** Genetic Algorithm, **ICFS:** Improved Correlation-based Feature Selection, **BPNN:** Backpropagation Neural Network, **RELS-TSVM:** Robust energy-based least squares twin SVM, **WELM:** Weighted Extreme Learning Machine, **sEEG:** scalp EEG, **iEEG:** intracranial EEG. **ACC:** Accuracy, **SN:** Sensitivity, **SP:** Specificity, **FAR:** False Aram Rate, **DL:** Detection Latency.

But, the effect of the relation between EEG and ECG on epilepsy and the firing location detection are not studied before based on our knowledge. This motivates us to develop a system based on the interaction between brain activity, measured by the EEG signals, and heart activity, measured by the ECG signal, for detecting epileptic seizures and the firing location. The challenge is how to develop a high precision and low complexity system to reach the average human performance with a detection rate of 65% and a false alarm rate of 12 alarms/24 hours [9].

Various technologies for determining the epileptic features have been developed and investigated in the literature based on EEG recordings [10]–[30], ECG recordings [31]–[33], or both ECG and EEG recordings [7], [8], [34] as listed in Table I. It is noticed that the extracted features in most of the previous work are based on time [11], [16], [20], [35] or/and frequency-domain [8], [12], [14], [15], [28], [29], [31], [32] which could not capture the behavior of the non-stationary recordings due to the wide variety of frequencies, amplitudes, spikes, and waves that can appear during the seizure onset time [10]. Moreover, most of existing methods cannot generate a general capability model for seizure detection because they depend on limited subjects datasets, no more than 24 patients, with only one seizure type (i.e. Bonn {10 subj./ 1 ch.} [36], CHB-MIT {22 subj./22 ch.} [37], Freiburg {21 subj./ 6 ch.} [38], and EPILEPSIAE{24 subj.} [39]). Furthermore, the detection of epilepsy firing location is not considered before according to our knowledge due to the unavailability of channel-based labeled datasets.

Even though the brain is the origin of epileptic discharges, these discharges lead to variations in cardiac autonomic nervous function which is transferred through sympathetic and parasympathetic nerves to the heart nervous system. This affects the heart operation in a way directly detected by the changes in the features of the ECG signal especially the heart rate variability (HRV) of epileptic patients [6], [40]. So, introducing Electrocardiograph (ECG) with EEG for detecting epileptic seizures can overcome the intolerance of EEG and improve the detection rate [7], [34] because ECG has distinctive, simple, and semi periodic features compared to EEG. Moreover, coupling the two signals shows the coincidental variations, the abnormal variations in EEG which coincide

with abnormal variations in the ECG. Therefore, the unrelated variations, such as artifacts or noise-related variations, have much less effective and can be filtered out. It is observed that the previous works depend on fusing either the extracted features or the classification results of EEG-only and ECG-only without considering the relation between the ECG and EEG signals. Therefore, the improvement in detection rate does not exceed 6% compared to using EEG signal as illustrated in [34].

All the above-mentioned shortcomings motivate us to develop a new method for detecting epileptic seizures and the firing location based on studying the frequency interaction of EEG signal and heart rate variability (HRV) of ECG signal, for simplicity we called it the Brain-Heart Interaction (BHI). BHI allows us to study the nonlinear coupling and variation of phase-synchronization [41], [42] between brain regions and the heart which are effective for distinguishing between ictal and interictal events. Calculating BHI between ECG and all EEG channels increases the system's complexity. Therefore, EEG channels are converted to only two surrogate channels representing the left and right brain hemispheres, and the BHI interactions are calculated between these two channels and ECG, resulting a low complexity system. In order to explain the effectiveness of using ECG, two cases are considered for detecting epileptic seizures, namely brain-components interaction (BI) and BHI.

In this paper, a new method based on BHI / BI is proposed for detecting epileptic seizures and determining the firing location across the EEG channels. In order to reduce the computational complexity, all channels of EEG recordings are converted to only two surrogate channels representing the left and right brain hemispheres during the seizure detection task. Also, the firing location is triggered only once the seizure onset is detected, resulting a low power system. Moreover, different classification networks based on combining Convolution Neural Network (CNN), Multi-Layer Perceptron (MLP), and Support Vector Machine (SVM) are constructed in this study. The largest available EEG/ECG dataset (TUSZ) [43] with 315 subjects and 7 seizure types is considered to evaluate the generalization capability of the proposed method. Based on the evaluation results, the proposed method outperforms the other methods [24], [25] by detecting more than 68% of epileptic seizures with 11.9 false alarms/24h. Moreover, the performance of the proposed method is superior to the average human performance (i.e., the sensitivity of 65% with 12 false alarms/24 h) based on the quantitative EEG (qEEG) tool [9].

The paper is organized as follows. Section II describes the considered database in this paper. The detail of the proposed method is presented in section III. Section IV explains the evaluation of the proposed method and presents the obtained results. Section V offers some conclusions and future work.

## II. EEG/ECG Dataset

The Temple University Hospital Seizure Detection Corpus (TUSZ) [43], [44] is the largest open-source EEG/ECG corpus for seizure detection and provides an accurate representation of actual clinical conditions. The last version of the TUSZ corpus (v1.5) contains over 315 patients with ages of 1∼ 90 years (51% female and 49% male). Each patient's record consists of 19 channel EEG recordings and one channel ECG recordings with a total record time of 797 hours for all patients. In particular, the TUSZ corpus is the only dataset that provides different types of epileptic seizure signal. This corpus contains 1791 labeled seizure events of 7 different seizure types with a total duration of 36 hours. The sampling frequency of the raw data varies from 250 Hz to 1 kHz. The overall and channel-based annotations of the seizure events are given for the Two Common Reference Points (TCP) montage of 22 channels.

For consistency consideration, the 19 channels of EEG recordings are converted into 22 channels of TCP montage according to the given annotations. Moreover, all data of the TUSZ corpus are resampled at 250 Hz. Finally, all labeled seizure events of 7 different seizure types are considered to design a general capability model.

## III. Methodology

Detecting epileptic discharges using all EEG channels is a time-consuming process and increases the system's complexity. Generally, the epileptic discharges start firing in a certain channel and then diffuse in all channels in the case of generalized seizures or diffuse in a limited number of channels in case of partial seizures. These discharges can occur in the left hemisphere or the right hemisphere or both [45]. So as to save computational time, the 22 channels of EEG recordings are converted into two surrogate channels using the average filter during the detection of epileptic seizures as shown in Fig. 1. These two channels represent the average of the 11 channels of the right hemisphere ($EEG_{RH}$, represented by the blue line in Fig.1) and the 11 channels of the left hemisphere ($EEG_{LH}$, represented by the green line in Fig.1), respectively.

Our idea for extracting the distinguishing features of epileptic seizures is based on studying the interaction between the two surrogate EEG signals and the HRV of the ECG signal. For each detected seizure, the system generates an alarm and triggers the firing location detector to find the location of firing across the 22 channels of EEG signal ($EEG_{ALL}$, represented by the black line in Fig.1) based on the interaction between each EEG channel and HRV of ECG. This saves the system's power because it processes and extracts features from all EEG channels only during the seizures onset time which is very small compared to the non-seizure time. The main stages of the proposed system are the preprocessing, the features extraction, and the classification stage.

### A. Preprocessing Stage

The total duration of seizure events in the TUSZ corpus is 36 hours compared to 761 hours of background data. Since the first 60 sec of an EEG recording is enough for identifying whether the patient has epilepsy or not [46], we used only the first 200 sec from each session of the background data during the model training to reduce the effect of the imbalanced data problem. To process and extract features of EEG/ECG recordings, a moving window is used. A 5-sec window is chosen to optimize the complexity and efficiency. To increase the seizure data samples and solve the imbalanced data problem, 50%

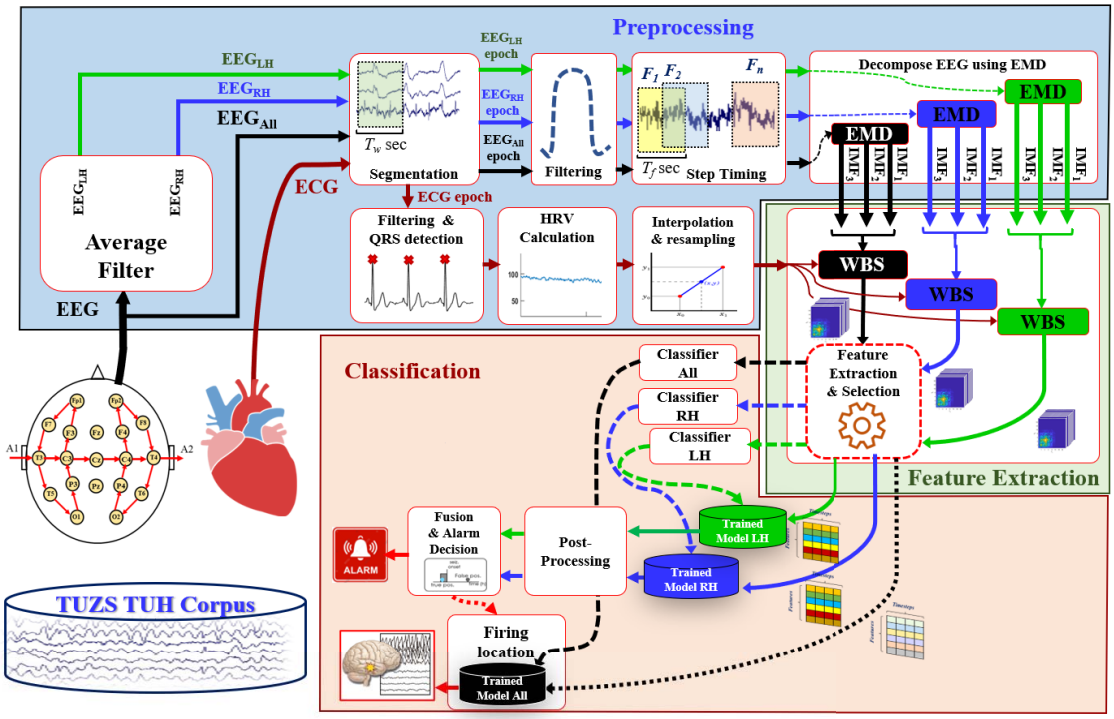


Fig. 1. Framework of the proposed seizure detection system. The proposed system consists of three main steps; preprocessing step, feature extraction step, and classification step. $EEG_{RH}$ is the surrogate channel of right brain hemisphere (represented by green line), $EEG_{LH}$ is the surrogate channel of left-brain hemisphere (represented by blue line), and $EEG_{ALL}$ are the 22 channels of EEG record (represented by black line).

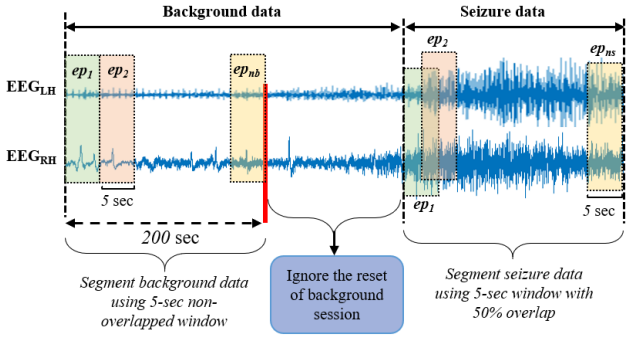


Fig. 2. Segmentation technique of background and seizure data. A nonoverlap 5-sec window is used for segmenting the background data and a 50% overlapped 5-sec window for segmenting the seizure data.

overlapped and non-overlapped 5-sec windows are used to segment the seizure and the background events of training data respectively into 5-sec epochs as shown in Fig. 2. However, in the testing process, a non-overlap 5-sec window is used to segment the input data into 5-sec epochs. The preprocessing detail of EEG and ECG epochs are explained below:

*1) EEG Preprocessing:* Each 5-sec epoch of EEG signal is filtered using an IIR elliptic bandpass filter with cutoff frequencies of [1 48] Hz to remove the unwanted frequencies, baseline wander, and power line noise. To monitor the transients of the epileptic discharges and extract temporal dependence features, each 5-sec EEG epoch is divided into $n$ frames (timesteps) using a 50% overlapped window with a duration of $T_f$. After that, each frame is decomposed into different components to study the interaction between them.

Currently, Empirical Mode Decomposition (EMD) [12], [47], Empirical Wavelet Transform (EWT) [48], variational mode decomposition [49], and iterative filtering [50] and their variants are popular adaptive decomposition algorithms. EMD, with its different versions, is one of the most commonly used methods for time-frequency analysis of the non-stationary and non-linear signals such as EEG, ECG, photoplethysmogram [51], etc. EMD describes the behavior of these signals by decomposing them into intrinsic mode functions (IMF) to obtain the instantaneous frequency of the intrinsic modes. EMD is preferred over WT when good time resolution is crucial, due to its instantaneous frequency property. Moreover, EMD does not need to be combined with other techniques to perform well and the adjustment of its algorithm's parameters is relatively simple [52]. So, EMD is utilized for decomposing the EEG signal into different IMF components. Since the bandpass filter removed the high-frequency noise of the EEG signal, the low IMF components contain most of the signal information. Therefore, we choose the first three IMF components (i.e., $IMF_1$, $IMF_2$, and $IMF_3$) that are holding the most energy for representing the EEG signal in this study.

*2) ECG Preprocessing:* To clean and detect the R peaks of each 5-sec ECG epoch, the Tompkins QRS detection algorithm [53] is used. Based on the detected RR-intervals, the HRV of the 5-sec ECG epoch is calculated by (1). The RR intervals are not equally spaced and HRV should have a fixed sampling frequency. Thus, the HRV values are interpolated

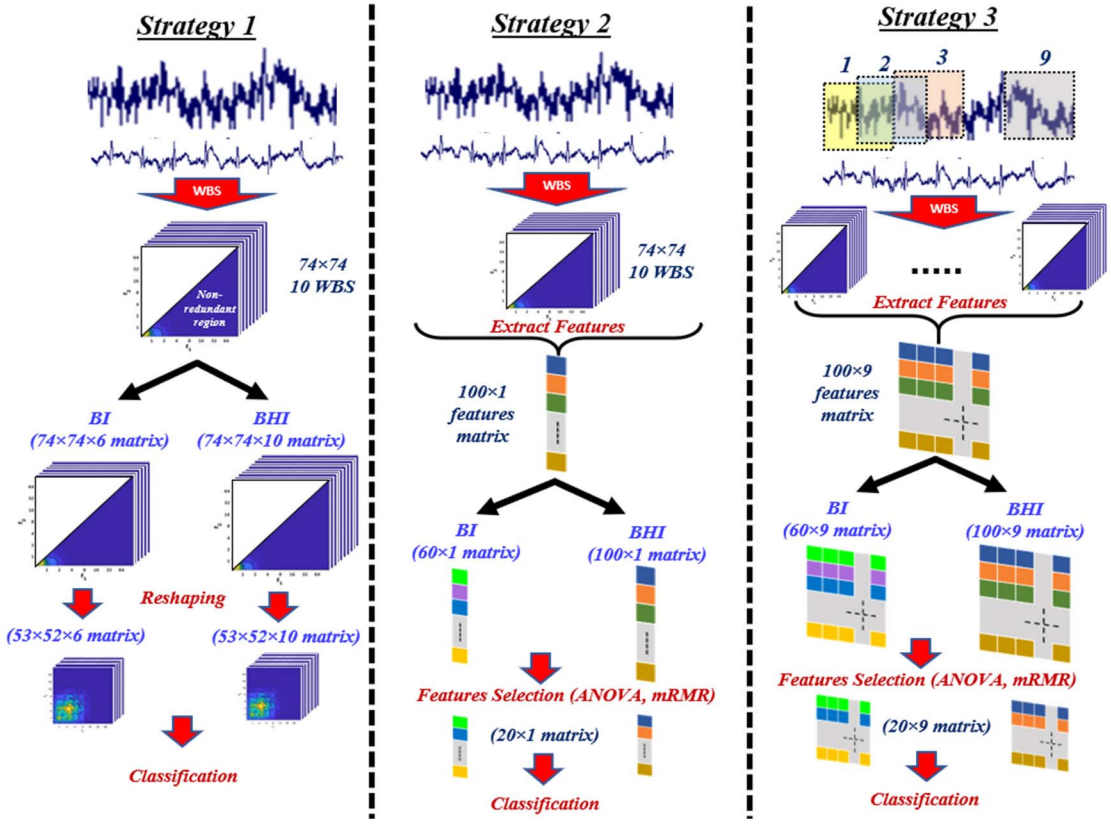


Fig. 3. The proposed three strategies of seizure detection. In strategy 1, the calculated WBS bi-spectrums are passed direct to the classification; while in strategies 2 and 3, 10 features are calculated for each WBS, and these features are passed to feature selection and then classification.

using a cubic spline interpolation technique [32] and the obtained signal is resampled at a certain sampling frequency to have the same length of EEG frame (i.e., $250 \times T_f$ samples).

$$HRV = \frac{60}{RR\ interval\ time\ series} \times sampling\_rate \quad (1)$$

## B. Feature Extraction Stage

Designing a high-precision system depends on extracting significant features that characterize epileptic discharges. Our approach is based on calculating the BHI interaction for extracting discriminative features. The Wavelet Bispectrum (WBS) [54], [55] method is utilized for calculating the BHI between the three IMF components of each $T_f$ sec frame of EEG signal and HRV of each 5-sec ECG epoch. As a result, 10 bi-spectrums with size 74 × 74 are formed, namely $WB_{IMF11}$, $WB_{IMF12}$, $WB_{IMF13}$, $WB_{IMF22}$, $WB_{IMF23}$, $WB_{IMF33}$, $WB_{IMF1-HRV}$, $WB_{IMF2-HRV}$, $WB_{IMF3-HRV}$, and $WB_{HRV-HRV}$. All 10 bi-spectrums are considered in the BHI case, while in the BI case only the first 6 bi-spectrums are considered. So as to find the effective technique for extracting the accurate epileptic features, three strategies are considered as demonstrated by Fig. 3:

1) ***Strategy 1:*** The 5-sec epoch of the EEG signal is considered as one frame (i.e. $T_f = 5$ sec) and 10 bi-spectrums with a size of $74 \times 74$ are calculated for which. Due to the symmetries of WBS, the non-redundant region ($\Omega$) of each WBS is reshaped as a matrix with a size of $53 \times 52$ to reduce the amount of data that is passed to the classification network. As a result, two 3D matrices of size $53 \times 52 \times 10$ and $53 \times 52 \times 6$ are considered for BHI and BI cases, respectively.
2) ***Strategy 2:*** The 5-sec EEG epoch is considered as one frame (i.e. $T_f = 5$ sec) and the 10 WBS bi-spectrums of BHI are calculated as in strategy 1. But instead of passing the WBS direct to the classification network, different features are extracted from the $\Omega$ region of each WBS and passed to the classification network. Some features considered in previous work [23], [56] with Fourier bi-spectrum, such as the bispectrum mean, the normalized bispectrum entropies and the phase entropy, are used to extract the quantitative and regularity information of each WBS. Moreover, other features such as the maximum magnitude, skewness, and kurtosis of the WBS, considered in our work before [41], are introduced to characterize the high correlation zone of each WBS. A total of 10 features are extracted from each calculated WBS as illustrated in Table II. As a result, a feature vector of size $100 \times 1$ is formed for each epoch. This corresponds to the dashed feature extraction block in Fig. 1. The whole feature vector of size $100 \times 1$ is used in the BHI case and only the first 60 features (i.e. $60 \times 1$) are considered in the BI case.
3) ***Strategy 3:*** The 5-sec EEG epoch is divided into 9 frames using a 50% overlapped 1-sec window

TABLE II
EXTRACTED FEATURES OF WBS FOR STRATEGIES 2 AND 3

| Feature | Equation | Feature | Equation |
|---|---|---|---|
| Mean magnitude of bispectrum | $X_{BS\_avg} = \frac{1}{L}\sum_{\Omega}\lvert WB(a_1,a_2)\rvert$ | Normalized bispectrum entropy | $X_{BS\_ent\,1} = -p_n \log p_n\,;\, p_n = \frac{\lvert WB(a_1,a_2)\rvert}{\sum_{\Omega}\lvert WB(a_1,a_2)\rvert}$ |
| Maximum magnitude of bispectrum | $X_{BS\_max} = \max(\lvert WB(a_1,a_2)\rvert)$ | Normalized bispectrum squared entropy | $X_{BS\_ent\,2} = -p_{ns} \log p_{ns}\,;\, p_{ns} = \frac{\lvert WB(a_1,a_2)\rvert^2}{\sum_{\Omega}\lvert WB(a_1,a_2)\rvert^2}$ |
| Location of the maximum magnitude of bispectrum: | $X_{BS\_loc} = loc(\max(\lvert WB(a_1,a_2)\rvert))$ | Normalized bispectrum cubic entropy | $X_{BS\_ent\,3} = -p_{nc} \log p_{nc}\,;\, p_{nc} = \frac{\lvert WB(a_1,a_2)\rvert^3}{\sum_{\Omega}\lvert WB(a_1,a_2)\rvert^3}$ |
| Skewness of magnitude bispectrum | $X_{BS\_skew} = \frac{1}{(L-1)\sigma_s^3}\sum_{\Omega}\left(real\left(WB(a_1,a_2)\right) - \mu_s\right)^3$ <br> $\mu_s = \frac{1}{L}\sum_{\Omega}\lvert WB(a_1,a_2)\rvert, \sigma_s = \frac{1}{L}\sum_{\Omega}(\lvert WB(a_1,a_2)\rvert - \mu_s)^2$ | Phase entropy | $X_{BS\_Pe} = \sum_{m} p(\psi_m) log(p(\psi_m))$ <br> $p(\psi_m) = \frac{1}{L}\sum_{\Omega} I(\phi(WB(a_1,a_2)) \in \psi_m) \qquad \psi_m = \left\{\phi \lvert -\pi + \frac{2\pi m}{M} \le \phi \le -\pi + \frac{2\pi(m+1)}{M}\right\}, m = 0,1,\dots,M-1$ |
| Kurtosis of magnitude bispectrum | $X_{BS\_kurt} = \frac{1}{(L-1)\sigma_s^4}\sum_{\Omega}\left(real\left(WB(a_1,a_2)\right) - \mu_s\right)^4$ | First-order spectral moment of magnitude of diagonal elements | $X_{BS\_FOSM} = \sum_{K=1}^{N} Klog(\lvert WB(a_K,a_K)\rvert)$ |

$\boldsymbol{L}$ is the number of points in the non-redundant region ($\Omega$); $\boldsymbol{WB(a_1,a_2)}$ represents the WBS matrix; $\boldsymbol{\phi}$ is the phase angle of the bispectrum; $\mathbf{I}(\boldsymbol{\phi})$ is an indicator function that gives 1 when the value of $\phi$ is within the range of bin $\psi_m$; $\boldsymbol{M}$ is the number of bins for $\psi_m$; $\boldsymbol{\mu_s}$ is the mean of the WBS, and $\boldsymbol{\sigma_s}$ is the variance of the WBS.

(i.e. $T_f$=*1 sec*) and 10 WBS are calculated for each frame. The same 10 features considered in strategy 2 are calculated for each WBS of each frame. As a result, a feature matrix of size $100\times9$ is formed, where the first dimension represents the number of extracted features of the calculated 10 WBS bi-spectrums and the second dimension is the number of frames within a 5-sec epoch. Extracting features from different timesteps (frames) allows the system to track the transient changes with keeping the temporal dependence of the epileptic seizures. The whole extracted features matrix is utilized for the BHI case, while the first $60\times9$ part of the feature matrix is considered in the BI case.

The extracted features in strategies 2 and 3 are normalized using Z-score [57] to have zero mean and unity standard deviation. Since not all extracted features are significant, the one-way ANOVA test is used to study the significance of the extracted features. The significant features should have $p$ values less than 0.05. Then, the Minimum Redundant and Maximum Relevant (MRMR) technique [58] is used for ranking the features according to their redundancy and relevance to the output, and only the top 20 features were selected in our study.

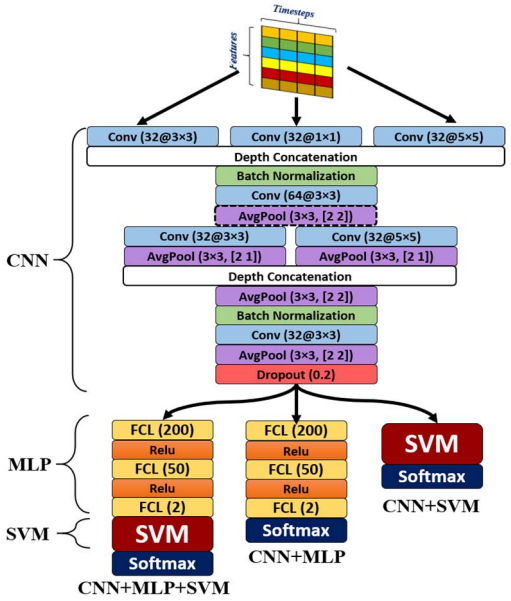


Fig. 4. The proposed classifier stuctures (CNN+SVM, CNN+MLP, and CNN+MLP+SVM); The dashed average-pooling layer is added only for strategy 1, the second dimention of kernal size and stide of all layer is set by 1 for strategy 2.

## C. Classification Stage

In this work, different classification architectures are optimized based on combining Convolutional Neural Network (CNN), Multi-Layer Perceptron (MLP), and Support Vector Machine (SVM).

*1) Classification Network Architectures:* The optimized architecture of the CNN network consists of 4 convolution layers, 2 batch normalization layers, 3 average-pooling layers, and one dropout layer as shown in Fig. 4. Each convolution layer consists of a Conv2D layer and a rectified linear units (ReLU) activation layer. The first and third convolution layers consist of three and two parallel branches with different kernel sizes respectively to extract different local features. ReLU activation function is used after each Cov2D layer to perform a threshold operation on each element because it is more effective than the sigmoid and hyperbolic tangent functions as proved in [59]. A batch normalization layer is used to normalize the distribution of features after ReLU not before to avoid the negative elements of convolution. To downsample the feature maps, an average-pooling layer is used after the activation layer. Finally, a dropout layer is utilized to reduce the overfitting problem.

The MLP structure consists of three Fully Connected Layers (FCL) with 200, 50, and 2 hidden units respectively. A ReLU activation function is used after each FCL layer

except the output layer. For the SVM classifier, the common Radial Basis kernel Function (RBF) is used to map the features vector from a low-dimensional space to a high-dimensional space. Three classification networks based on combining CNN, MLP, and SVM are constructed as demonstrated in Fig. 4. The first classification network is based on combining CNN and MLP (*i.e. CNN+MLP classifier*). The second classification network depended on replacing the MLP after CNN was well trained by the SVM classifier (*i.e. CNN+SVM classifier*). Inserting the SVM classifier before the softmax layer of the first classification network after being well-trained forms the third classification network (*i.e. CNN+MLP+SVM classifier*). A softmax layer is used at the output of the three constructed classifiers for calculating the probability values of seizure ($P_{seiz}$) and background ($P_{back}$) events. The details of kernel size, stride, and the number of kernels for each strategy are mentioned in Fig. 4. For strategy 2, the second dimension of kernel size and stride in Conv and average-pooling layers are set by 1 because the input data to the classifier is a vector (i.e. 1-D). An additional average-pooling layer, shown in Fig. 4 by the dashed box, is added to the classifier for strategy 1 to reduce the dimension of the feature map because the input data size is larger compared to the other strategies.

The CNN+MLP classifier is trained using the adaptive moment estimation (ADAM) training algorithm with the hyperparameters such as learning rate is 0.0008 which is dropped out by a factor of 0.5 after every 5 epochs, decay factors of gradient and squared gradient are 0.9 and 0.999 respectively, epsilon is $10^{-8}$ for numerical stability and the mini-batch size is set to 512. The cross-entropy is used as a loss function and the maximum number of epochs is 30.

*2) Post-Processing and Alarm Decision:* In the real-time system, a post-processing algorithm is used for processing the outputs of classifiers and reducing the number of false alarms. The output of the softmax layer is a vector of two probability values $[P_{seiz}\, P_{back}]$ for seizure and background events. If $P_{seiz}$ of an epoch is greater than $P_{th}$, we consider this epoch as a suspected seizure; otherwise, it is detected as a background epoch. Increasing the value of $P_{th}$ improves the FAR at the expense of reducing sensitivity and vice versa. So, the value of $P_{th}$ is set by 0.65 to tradeoff between FAR and sensitivity. For each epoch suspected to point to a seizure state, a post-processing algorithm is used to decide the state of the current epoch as a seizure if the state of the previous or next epoch to it is a seizure; otherwise, it is considered as a normal state. Although this procedure adds a latency of 5-sec to the processing time, the post-processing smooths the outputs of classifiers to improve the FAR and sensitivity of the system.

The final decision of each epoch is decided based on fusing the classification outputs of both $EEG_{RH}$ and $EEG_{LH}$ classifiers. The fusion function that is considered in this study is the OR function since the seizure can happen on the right-brain hemisphere or the left-brain hemisphere or both. Moreover, to reduce the number of consecutive false alarms, the seizure density function, which varies between 0 and 1 over the duration of the record, is considered for taking the alarm decision of the detected seizure as described in [60]. An event is detected as a seizure event if the average value of seizure density function over the event duration exceeds a seizure density threshold ($SD_{th}$) and is detected as a background event otherwise.

*3) Determination of Firing Location:* Determining the seizure firing location in the brain can help clinicians for diagnosing epileptic seizures. After detecting the onset seizure time, we go across the 22 channels of EEG signal ($EEG_{ALL}$) to find the firing location using the firing location classifier. The classification network of the firing location is triggered only if the epoch is detected as a seizure event as illustrated in Fig. 1 to save computational time and power of the system. For each detected seizure epoch, the firing location classifier detects the EEG channels of seizure firing based on the bispectrum interaction of each EEG channel and/or the HRV of the ECG signal.

*4) Performance Metrics:* Different metrics such as Accuracy (ACC), Sensitivity (Sen), Specificity (Spec), Precision (Prec), and F1-Score considered in [41] are used for measuring the performance of the system based on the classification outputs, i.e. TP, TN, FP, and FN. Other metrics such as False Alarm Rate (FAR, definition 1) and Detection Latency (DL, definition 2) are introduced to measure the robustness of the proposed algorithm.

***Definition 1*** *False Alarm Rate (FAR /24 hours):* A false alarm occurs if the integral of seizure density function over a background event exceeds $SD_{th}$. The ratio between the number of false alarms and the duration of the EEG recorded over 24 hours is defined as a False Alarm Rate per 24 hours (*FAR/24h= No. of false alarms / total record duration per 24 h*)

***Definition 2*** *Detection Latency (DL sec):* is the delay between the electrographic seizure onset marked by the clinicians and a seizure onset detected by the proposed technique.

Where, TP (True Positive) is the total number of correct seizure event detections that have average seizure density exceed $SD_{th}$, TN (True Negative) is the total number of correct background event detections that have average seizure density fall below $SD_{th}$, FP (False Positive) and FN (False Negative) are the total number of events that are detected as a seizure and a background accidentally, respectively.

## IV. Results and Discussion

The TUSZ dataset is used for training and testing the structured classification networks. The training and testing datasets of the TUSZ corpus are shuffled to balance the proportion of different classes of epileptic events in the training (DS1) and testing (DS2) sets while keeping the same ratio between the size of two sets as the original sets as illustrated in Fig. 5. Table III lists the 5-sec epochs of background and seizure data for $EEG_{LH}$ and $EEG_{RH}$ of DS1 and DS2. Due to the imbalanced data size of different events as illustrated in Table III, a resampling technique [61] is used to increase the training samples of the seizure class and decrease the samples of the background class of DS1 before training the network. A 5-fold cross-validation method is used for dividing the DS1 into 80% and 20% for training and validating the model respectively through 5 iterations. While the DS2 is used for testing the network at each iteration and the average

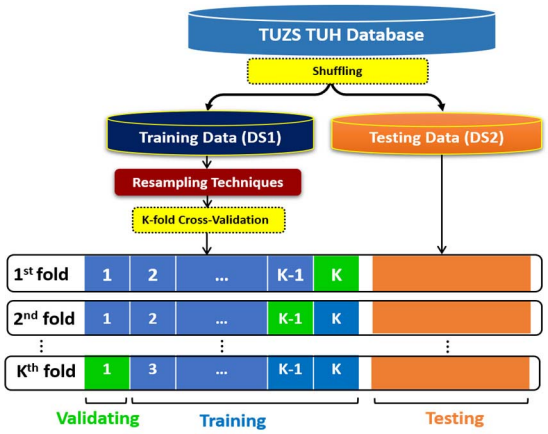


Fig. 5. Preparing data for training and testing using k-fold cross-validation, the training set is resampled to balance data of each class before training.

TABLE III
DISTRIBUTION OF 5-SEC EPOCHS FOR TRAIN AND TEST SETS OF TUSZ

| | $EEG_{LH}$ | | $EEG_{RH}$ | |
|---|---|---|---|---|
| | Background (Negative) | Seizure (Positive) | Background (Negative) | Seizure (Positive) |
| Train set (DS1) | 124,391 | 30,816 | 126,632 | 28,575 |
| Test set (DS2) | 41,683 | 18,794 | 44,686 | 15,791 |

of the obtained accuracy, F1-score, sensitivity (Sen), and specificity (Spec) for the 5 iterations were taken as the final results.

Different values of $SD_{th}$ are considered to measure the performance of the proposed system for detecting epileptic seizures. Figs. 6-8 show the Detection Error Tradeoff curves (DET) of the three classification structures for all strategies. In the case of the CNN+MLP classifier, it is observed from Fig. 6 that strategy 3 has the best results for the BHI and BI cases compared to the other strategies while the BI case in strategy 2 has the worst results. Considering the BHI interaction improved the performance of the proposed system for strategies 2 and 3 compared to the BI case. The sensitivity results of the BHI case of strategy 3 are improved by 47% and 15% at FAR of 4 and 7 /24 h, respectively, while the FAR values are dropped by 39% and 3% at a Sen of 30% and 66.7% respectively.

According to the DET results of the CNN+SVM classifier (see Fig. 7), utilizing the BHI interaction improved the performance of the system compared to the BI for all strategies. It is noticed that strategy 3 gives the best results and strategy 2 gives the worst results. For strategy 3, BHI improves the sensitivity by 44%, 6%, and 2.4 % at FAR of 4, 7, and 12 /24h and improves the FAR by 18 % at a Sen of 30% compared to the BI case. While in the case of the CNN+MLP+SVM classifier, Fig. 8, the BHI improves the results of strategies 2 and 3 compared to the BI case of the same strategies. In strategy 3, the Sen results of the BHI case are enhanced by 48%, 18%, and 2% at FAR of 4, 7, and 12 /24h compared to the BI case.

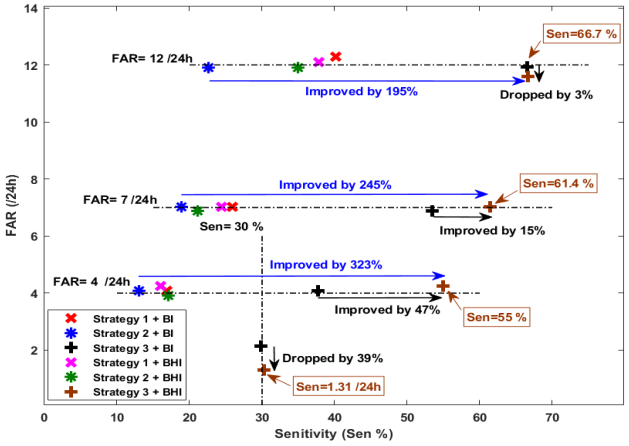


Fig. 6. DET of CNN+MLP classifier for all 3 strategies using BHI and BI.

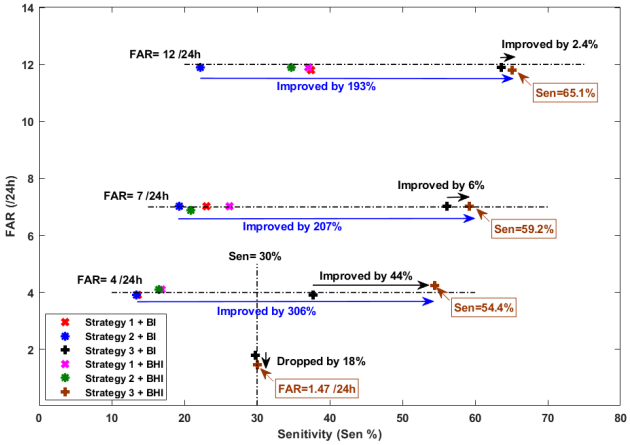


Fig. 7. DET of CNN+SVM classifier for all 3 strategies using BHI and BI.

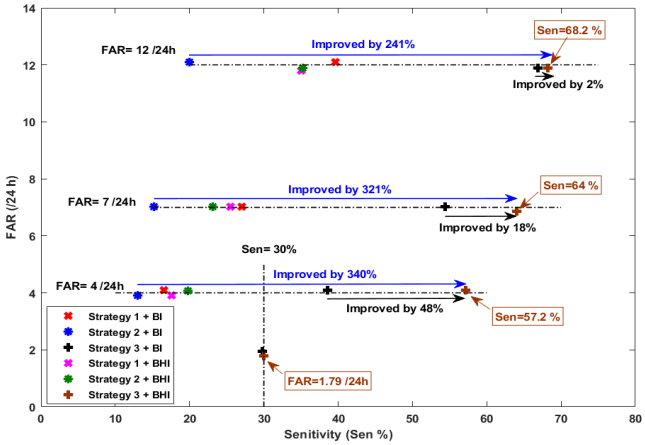


Fig. 8. DET of CNN+MLP+SVM classifier for all 3 strategies using BHI and BI.

From figures 6-8, it is observed that dividing the 5-sec EEG epoch into 9 frames in strategy 3 allows the network to extract the local and temporal dependence features, resulting in the performance being improved. While considering the 5-sec EEG epoch as one frame in strategies 1 and 2 does not allow the network to extract the temporal dependence

TABLE IV
COMPARISON OF THE PROPOSED STRATEGIES WITH THE STATE-OF-ART METHODS

| Method | | | $SD_{th}$ | Sen (%) | | | Spec (%) | | | FAR (/24h) | | | DL (sec) | | |
|---|---|---|---|---|---|---|---|---|---|---|---|---|---|---|---|
| Deep Learning Methods [24] | | HMM | - | 30.32 | | | 80.07 | | | 244 | | | NA | | |
| | | HMM/SdA | - | 35.35 | | | 73.35 | | | 77 | | | | | |
| | | HMM/LSTM | - | 30.05 | | | 80.53 | | | 60 | | | | | |
| | | IPCA/LSTM | - | 32.97 | | | 77.57 | | | 73 | | | | | |
| | | CNN/MLP | - | 39.09 | | | 76.84 | | | 77 | | | | | |
| | | CNN/LSTM | - | 30.83 | | | 96.86 | | | 7 | | | | | |
| DWT-Net (5-sec window) [25] | | | 0.76 | 30.25 | | | 96.64 | | | 4 | | | | | |
| | | | 0.35 | 59.07 | | | 89.72 | | | 12 | | | | | |
| Our Work | Brain Interaction () | CNN+MLP | - | - | 0.86 | - | - | **29.8** | - | - | **99.0** | - | - | **2.13** | 9.33 | 24.35 | 10.62 |
| | | | 0.98 | 0.20 | 0.79 | 16.9 | 13.0 | **37.7** | 98.1 | 98.1 | **98.1** | 4.09 | 4.09 | **4.09** | | | |
| | | | 0.91 | 0.15 | 0.63 | 25.9 | 18.9 | **53.5** | 96.8 | 96.8 | **96.9** | 7.03 | 7.03 | **6.87** | | | |
| | | | 0.80 | 0.09 | 0.49 | 40.2 | 22.6 | **66.5** | 94.4 | 94.6 | **94.6** | 12.3 | 11.9 | **11.93** | | | |
| | | CNN+SVM | - | - | 0.88 | - | - | **29.8** | - | - | **99.2** | - | - | **1.79** | 11.47 | 28.70 | 10.09 |
| | | | 0.94 | 0.20 | 0.80 | 13.6 | 13.4 | **37.7** | 98.2 | 98.2 | **98.2** | 3.92 | 3.92 | **3.92** | | | |
| | | | 0.84 | 0.15 | 0.65 | 23.0 | 19.3 | **56.1** | 96.8 | 96.8 | **96.8** | 7.03 | 7.03 | **7.03** | | | |
| | | | 0.72 | 0.10 | 0.53 | 37.4 | 22.2 | **63.6** | 94.6 | 94.6 | **94.6** | 11.8 | 11.9 | **11.9** | | | |
| | | CNN+MLP+ SVM | - | - | 0.87 | - | - | **29.8** | - | - | **99.1** | - | - | **1.96** | 9.68 | 27.31 | 10.63 |
| | | | 0.98 | 0.33 | 0.78 | 16.5 | 13.0 | **38.6** | 98.1 | 98.2 | **98.1** | 4.09 | 3.92 | **4.09** | | | |
| | | | 0.89 | 0.28 | 0.62 | 27.0 | 15.2 | **54.4** | 96.8 | 96.8 | **96.8** | 7.03 | 7.03 | **7.03** | | | |
| | | | 0.79 | 0.20 | 0.49 | 39.6 | 20.0 | **66.9** | 94.5 | 94.5 | **94.6** | 12.1 | 12.1 | **11.9** | | | |
| | Brain-heart Interaction (BHI) | CNN+MLP | - | - | 0.88 | - | - | **30.3** | - | - | **99.4** | - | - | **1.31** | 8.77 | 29.83 | 12.00 |
| | | | 0.95 | 0.75 | 0.67 | 16.0 | 17.1 | **55.0** | 98 | 98.2 | **98.1** | 4.25 | 3.92 | **4.25** | | | |
| | | | 0.88 | 0.67 | 0.55 | 24.4 | 21.1 | **61.4** | 96.8 | 96.9 | **96.8** | 7.03 | 6.87 | **7.03** | | | |
| | | | 0.80 | 0.45 | 0.45 | 37.8 | 35.0 | **66.7** | 94.6 | 94.6 | **94.7** | 12.1 | 11.9 | **11.6** | | | |
| | | CNN+SVM | | - | 0.88 | - | - | **30.0** | - | - | **99.3** | - | - | **1.47** | 10.97 | 28.06 | 12.28 |
| | | | 0.90 | 0.73 | 0.67 | 16.9 | 16.5 | **54.4** | 98.1 | 98.1 | **98.1** | 4.09 | 4.09 | **4.25** | | | |
| | | | 0.81 | 0.63 | 0.56 | 26.2 | 20.9 | **59.2** | 96.8 | 96.8 | **96.8** | 7.03 | 6.87 | **7.03** | | | |
| | | | 0.73 | 0.39 | 0.47 | 37.1 | 34.7 | **65.1** | 94.6 | 94.6 | **94.6** | 11.9 | 11.9 | **11.8** | | | |
| | | CNN+MLP+ SVM | - | - | 0.87 | - | - | **30.0** | - | - | **99.2** | - | - | **1.79** | 8.38 | 28.56 | 11.94 |
| | | | 0.97 | 0.72 | 0.65 | 17.6 | 19.8 | **57.2** | 98.2 | 98.1 | **98.1** | 3.92 | 4.07 | **4.09** | | | |
| | | | 0.89 | 0.66 | 0.53 | 25.5 | 23.1 | **64.0** | 96.8 | 96.8 | **96.9** | 7.03 | 7.03 | **6.87** | | | |
| | | | 0.82 | 0.42 | 0.44 | 35 | 35.2 | **68.2** | 94.6 | 94.6 | **94.6** | 11.8 | 11.9 | **11.9** | | | |
| Strategy | | | **1** | **2** | **3** | **1** | **2** | **3** | **1** | **2** | **3** | **1** | **2** | **3** | **1** | **2** | **3** |

features as a result the performance is degraded. Moreover, it is noticed that the BHI of strategy 3 is the best case while the BI of strategy 2 is the worst case for the three classification structures. This proved the effectiveness of using ECG with EEG for detecting epileptic seizures. Compared to the worst case, the Sen results of the best case are improved by a factor of 3.23, 2.45, and 1.95 for the CNN+MLP, by 3.06, 2.07, and 1.93 for the CNN+SVM, and by 3.40, 3.21, and 2.41 for the CNN+MLP+SVM at FAR of 4, 7, and 12 /24h, respectively. This confirms that considering SVM after the MLP network improves the system performance compared to other networks because the SVM maps the features vector of MLP from a low-dimensional space to a high-dimensional space.

Table IV shows the details of the obtained results compared to the results of Refs [24], [25] that used the TUSZ dataset. It is observed that strategy 3 outperforms the other methods because it can track the feature variation through the different time frames within each epoch. Moreover, increasing the value of $SD_{th}$ helps the system to combine several consecutive false alarms, which improves the FAR but decreases the system sensitivity. Fig. 9 shows the results of strategy 3 for all classification structures and results of Refs. [24], [25]. It is obvious that strategy 3 for all classification structures outperforms the performance of the average human detector based on the qEEG tool [9] by detecting more than 68% of seizure events with a FAR of 12/24h. The highest Sen of 68.2% with a FAR of 11.9/24h is achieved using the CNN+MLP+SVM structure

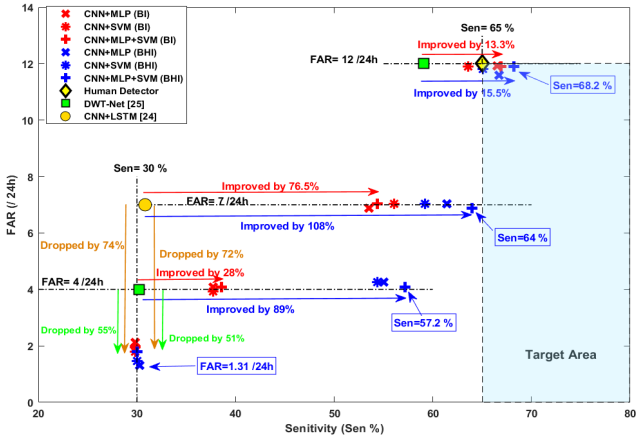


Fig. 9. Comparison of the proposed strategy 3 and the other methods.

with the BHI case, while the lowest FAR of 1.31/24h at a Sen of 30 % is achieved using the CNN+MLP structure with BHI case. Moreover, the DL results of strategies 1 and 3 outperform the results of strategy 2. The obtained values of DL change as 8.38 $\sim$ 11.47 sec and 10.09 $\sim$12.28 sec for strategies 1 and 3, respectively. Although BHI improves the FAR and Sen compared to BI, it slightly increases DL because the cardiac effects of epileptic discharges happen after the seizure onset.

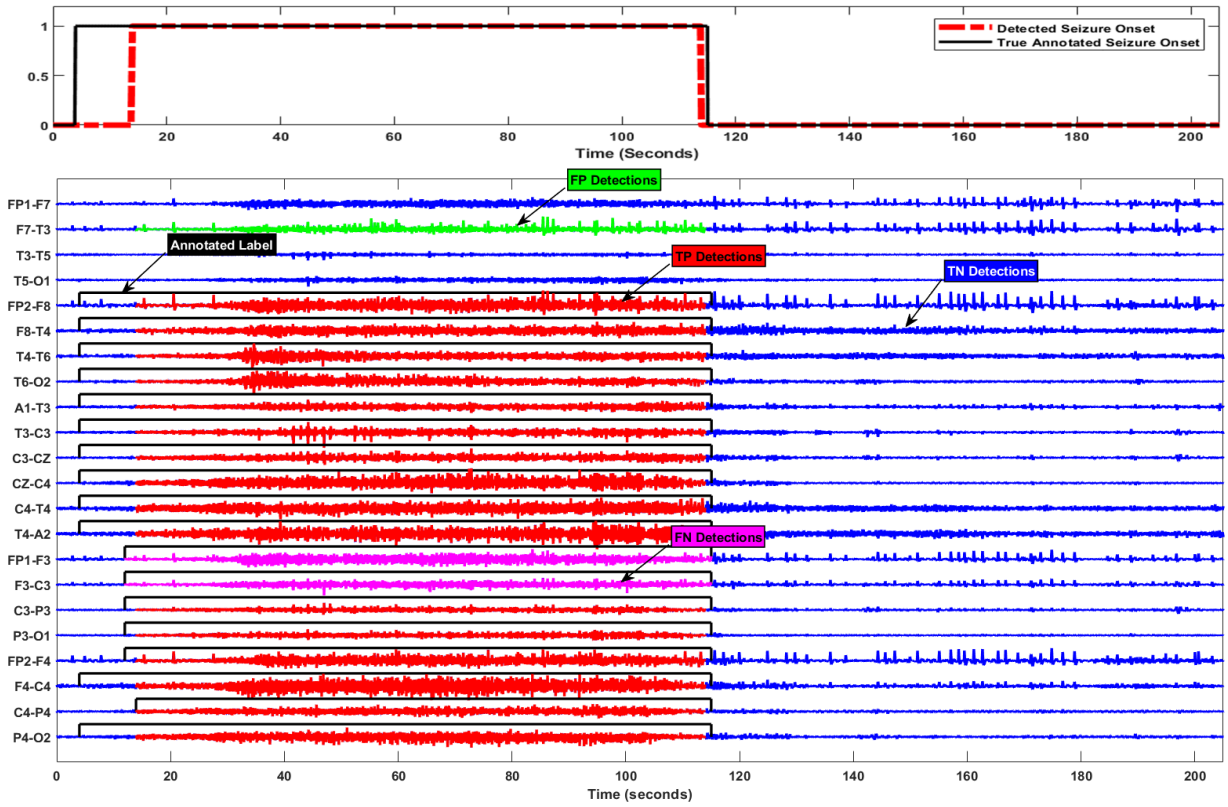


Fig. 10. Example 1 from TUZS corpus for detecting the seizure onset across the EEG channels.

For a fair comparison with other methods, the BI case is considered to measure the performance of the proposed method based on using EEG only. In the BI case, the CNN+MLP+SVM structure of strategy 3 enhances the sensitivity by 76.5% at FAR of 7 /24h compared to CNN/LSTM [24] and by 28% and 13.3% compared to DWT-Net [25] at 4 and 7 /24h, respectively. This proved that our method which used only two surrogate EEG channels outperforms the other methods which were based on all EEG channels. Also, introducing the ECG signal with EEG improves the detection rate. The CNN+MLP+SVM structure in the BHI case of strategy 3 improves the system's sensitivity and specificity by 108% and 0.04% at FAR of 7 /24h compared to CNN/LSTM of Ref. [24]. Also, it enhanced the sensitivity by 89% and 15.5% and the specificity by 1.5% and 5.44% at FAR of 4 and 12 /24h, respectively compared to DWT-Net [25]. Given the same sensitivity of 30%, the proposed system improves the FAR by 55% and 74% compared to DWT-Net and CNN/LSTM, respectively. This clarifies that the interaction between the brain and the heart (BHI case) improves the performance of the system compared to considering brain interaction (BI case) only.

Figs. 10-11 show two examples from DS2 of the TUSZ corpus for detecting the seizure onset and the firing channels by the proposed system. For the EEG record shown in Fig. 10, the overall seizure onset started after 4 sec, with respect to the beginning of the record, and lasted for 111 sec, and occurred across all channels except the first 4 channels according to the annotated label of the TUSZ dataset. It is observed that the proposed method detected the overall seizure onset with a DL of 9 sec referred to the annotated label. Across the channels of EEG, the proposed system detected the epileptic seizures of 16 channels correctly and missed only the FP1-F3 and F3-C3 channels, while the F7-T3 channel was mistakenly detected. In the second record sample shown in Fig. 11, the overall seizure onset started after 208 sec for a duration of 100 sec and occurred only on four channels of the right hemisphere channels, namely F8-T4, T4-T6, C4-T4, and T4-A2 channels. The proposed system detected the seizure onset correctly across the four channels with a DL of 14 sec as per the annotated label, and only one channel was mistakenly detected.

For the complexity aspect, converting the 22 channels of EEG into two surrogate channels reduces the computational complexity of the proposed system. Also, using simple signal processing methods like EMD and WBS fasts the proposed system. Moreover, our network structures are simple and have the smallest number of parameters compared to the other methods as illustrated in Table V. The model of strategy 3 has 213K parameters compared to 240K and 4.7M parameters of [24] and [25], respectively. For our implementation using MATLAB 2019a, the proposed three strategies require 17.3 sec, 1.46 sec, 1.26 sec respectively on a Desktop with an Intel®Core™i5-7500 3.4 GHz processor and 16 GB RAM for detecting 5-sec epoch at a sampling rate of 250 Hz. It is observed that dividing a 5-sec epoch into 1-sec frames in strategy 3 fasts the computational processes because it deals with a short duration signal compared to the other two strategies.

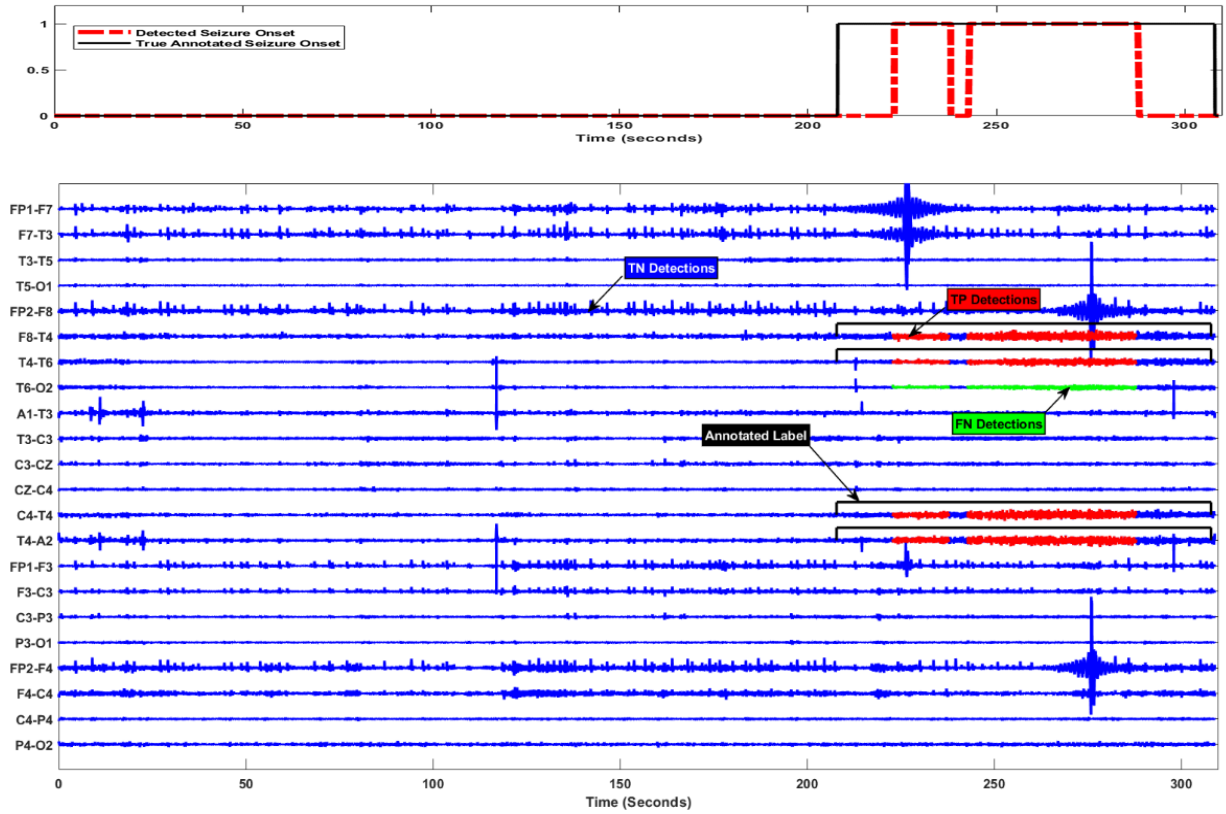


Fig. 11. Example 2 from TUZS corpus for detecting the seizure onset across the EEG channels.

TABLE V
NETWORK COMPLEXITY OF THE PROPOSED METHOD

| | (CNN/LSTM) [24] | DWT-Net [25] | Our work | | |
|---|---|---|---|---|---|
| | | | Strategy 1 | Strategy 2 | Strategy 3 |
| **Network Parameters** | 4,667,680 | 242,896 | 240,944 | 84,176 | **213,008** |

The advantages of the proposed framework can be summarized as 1) It is the first system for detecting epileptic seizures based on the interaction between the ECG and EEG signals; 2) It saves the computational complexity by reducing the channels of EEG signal to only two channels; 3) It can detect the seizure onset and also the firing location in the brain, and 4) It outperforms the human performance based on the qEEG tool by detecting more than 68% with 11.9 false alarms/ 24 hours and a detection latency of 11.94 sec. However, converting the 22 channels into 2 surrogate channels using the average filter causes a loss of information depending on the number of channels that seizure diffused through them. In the case of generalized seizures, the whole brain is affected, so the detection task won't be affected by the information loss due to channel converting. Also in partial seizures, which affect a lobe of the brain, the information loss of channel converting does not affect the detection performance because most of these partial seizures often spread to involve other lobes in the brain. For the limited diffused partial seizures (i.e., the seizure happens at one or two EEG channels), which are rarely happened, the surrogate channels can be increased to four to reduce the information loss.

## V. CONCLUSION

In this paper, a new method based on the brain-heart interaction is proposed for detecting epileptic seizures and the firing locations by incorporating the empirical mode decomposition and the wavelet bi-spectrum techniques. In the proposed method, the EEG channels are mapped into two surrogate channels incorporating with the ECG signal for detecting epileptic seizures to save the computational complexity. Three strategies are considered to find the effective technique for extracting accurate features. Also, three classification networks are constructed to classify the extracted features. The largest available EEG/ECG dataset (TUSZ) with 315 subjects and 7 seizure types is considered to measure the generalization capability of the proposed method. The obtained results confirmed that considering the brain-heart interaction improved the system performance compared to the brain frequency interaction because EEG is a weak and noisy signal. Furthermore, the proposed system outperforms the existing methods and human performance based on the qEEG tool by detecting more than 68% with 11.9 false alarms/ 24 hours and a detection latency of 11.94 sec. Future work should be continued to improve the ability of the proposed system to detect the limited diffused partial seizures by reducing the information loss due to converting the EEG channels into two surrogate channels. Moreover, studying the effect of training data size on the system performance.

## REFERENCES


[1] *Regional Office for the Western, Epilepsy in the Western Pacific Region: A Call to Action: Global Campaign Against Epilepsy*, WHO Regional Office for the Western Pacific, P. World Health Organization, Manila, Philippines, 2004.

[2] Y. Ge *et al.*, "Incidence of sudden unexpected death in epilepsy in community-based cohort in China," *Epilepsy Behav.*, vol. 76, pp. 76–83, Nov. 2017.

[3] S. Noachtar and J. Rémi, "The role of EEG in epilepsy: A critical review," *Epilepsy Behav.*, vol. 15, pp. 22–33, May 2009.

[4] W. O. Tatum *et al.*, "Clinical utility of EEG in diagnosing and monitoring epilepsy in adults," *Clin. Neurophysiol.*, vol. 129, no. 5, pp. 1056–1082, May 2018.

[5] C. Zhang, N. Sabor, J. Luo, Y. Pu, G. Wang, and Y. Lian, "Automatic removal of multiple artifacts for single-channel EEG," *J. Shanghai Jiaotong Univ. Sci.*, Oct. 2021, pp. 1–15.

[6] A. Popov, O. Panichev, Y. Karplyuk, Y. Smirnov, S. Zaunseder, and V. Kharytonov, "Heart beat-to-beat intervals classification for epileptic seizure prediction," in *Proc. Signal Process. Symp. (SPSympo)*, Sep. 2017, pp. 1–4.

[7] M. Qaraqe, M. Ismail, E. Serpedin, and H. Zulfi, "Epileptic seizure onset detection based on EEG and ECG data fusion," *Epilepsy Behav.*, vol. 58, pp. 48–60, May 2016.

[8] B. R. Greene, G. B. Boylan, R. B. Reilly, P. de Chazal, and S. Connolly, "Combination of EEG and ECG for improved automatic neonatal seizure detection," *Clin. Neurophysiol.*, vol. 118, no. 6, pp. 1348–1359, Jun. 2007.

[9] C. B. Swisher *et al.*, "Diagnostic accuracy of electrographic seizure detection by neurophysiologists and non-neurophysiologists in the adult ICU using a panel of quantitative EEG trends," *J. Clin. Neurophysiol.*, vol. 32, pp. 1348–1359, Aug. 2015.

[10] L. Boubchir, S. Al-Maadeed, A. Bouridane, and A. A. Chérif, "Time-frequency image descriptors-based features for EEG epileptic seizure activities detection and classification," presented at the IEEE Int. Conf. Acoust., Speech Signal Process. (ICASSP), South Brisbane, QLD, Australia, 2015.

[11] E. Tessy, P. P. M. Shanir, and S. Manafuddin, "Time domain analysis of epileptic EEG for seizure detection," in *Proc. Int. Conf. Next Gener. Intell. Syst. (ICNGIS)*, Sep. 2016.

[12] F. Riaz, A. Hassan, S. Rehman, I. K. Niazi, and K. Dremstrup, "EMD-based temporal and spectral features for the classification of EEG signals using supervised learning," *IEEE Trans. Neural Syst. Rehabil. Eng.*, vol. 24, no. 1, pp. 28–35, Jan. 2015.

[13] O. Kocadagli and R. Langari, "Classification of EEG signals for epileptic seizures using hybrid artificial neural networks based wavelet transforms and fuzzy relations," *Expert Syst. Appl.*, vol. 88, pp. 419–434, Dec. 2017.

[14] M. Mursalin, Y. Zhang, Y. Chen, and N. V. Chawla, "Automated epileptic seizure detection using improved correlation-based feature selection with random forest classifier," *Neurocomputing*, vol. 241, pp. 204–214, Jun. 2017.

[15] T. Zhang and W. Z. Chen, "LMD based features for the automatic seizure detection of EEG signals using SVM," *IEEE Trans. Neural Syst. Rehabil. Eng.*, vol. 25, no. 8, pp. 1100–1108, Aug. 2017.

[16] H. Zhang, Q. Meng, B. Meng, M. Liu, and Y. Li, "Epileptic seizure detection based on time domain features and weighted complex network," presented at the Intell. Comput. Theories Appl. ICIC, in Lecture Notes in Computer Science. Cham, Switzerland: Springer, 2018.

[17] M. Tanveer, R. B. Pachori, and N. V. Angami, "Entropy based features in FAWT framework for automated detection of epileptic seizure EEG signals," in *Proc. IEEE Symp. Ser. Comput. Intell. (SSCI)*, Nov. 2018, pp. 1946–1952.

[18] A. I. Sharaf, M. A. El-Soud, and I. M. El-Henawy, "An automated approach for epilepsy detection based on tunable Q-wavelet and firefly feature selection algorithm," *Int. J. Biomed. Imag.*, vol. 2018, pp. 1–12, Sep. 2018.

[19] H. R. Al Ghayab, Y. Li, S. Siuly, and S. Abdulla, "A feature extraction technique based on tunable Q-factor wavelet transform for brain signal classification," *J. Neurosci. Methods*, vol. 312, pp. 43–52, Jan. 2019.

[20] A. Baldominos and C. Ramon-Lozano, "Optimizing EEG energy-based seizure detection using genetic algorithms," in *Proc. IEEE Congr. Evol. Comput. (CEC)*, Jun. 2017, pp. 2338–2345.

[21] Q. Yuan *et al.*, "Epileptic seizure detection based on imbalanced classification and wavelet packet transform," *Seizure*, vol. 50, pp. 99–108, Aug. 2017.

[22] K. D. Tzimourta, A. T. Tzallas, N. Giannakeas, L. G. Astrakas, D. G. Tsalikakis, and M. G. Tsipouras, "Epileptic seizures classification based on long-term EEG signal wavelet analysis," presented at the Precis. Med. Powered by pHealth and Connected Health, Singapore, 2018.

[23] N. Mahmoodian, A. Boese, M. Friebe, and J. Haddadnia, "Epileptic seizure detection using cross-bispectrum of electroencephalogram signal," *Seizure*, vol. 66, pp. 4–11, Mar. 2019.

[24] M. Golmohammadi, S. Ziyabari, V. Shah, I. Obeid, and J. Picone, "Deep architectures for spatio-temporal modeling: Automated seizure detection in scalp EEGs," in *Proc. 17th IEEE Int. Conf. Mach. Learn. Appl. (ICMLA)*, Dec. 2018, pp. 745–750.

[25] Z. Zhang *et al.*, "DWT-Net: Seizure detection system with structured EEG montage and multiple feature extractor in convolution neural network," *J. Sensors*, vol. 2020, pp. 1–13, Aug. 2020.

[26] Y. Lu, Y. Ma, C. Chen, and Y. Wang, "Classification of single-channel EEG signals for epileptic seizures detection based on hybrid features," *Technol. Health Care*, vol. 26, no. S1, pp. 337–346, Jan. 2018.

[27] M. S. J. Solaija, S. Saleem, K. Khurshid, S. A. Hassan, and A. M. Kamboh, "Dynamic mode decomposition based epileptic seizure detection from scalp EEG," *IEEE Access*, vol. 6, pp. 38683–38692, 2018.

[28] L. S. Vidyaratne and K. M. Iftekharuddin, "Real-time epileptic seizure detection using EEG," *IEEE Trans. Neural Syst. Rehabil. Eng.*, vol. 25, no. 11, pp. 2146–2156, Nov. 2017.

[29] D. Wu *et al.*, "Automatic epileptic seizures joint detection algorithm based on improved multi-domain feature of cEEG and spike feature of aEEG," *IEEE Access*, vol. 7, pp. 41551–41564, 2019.

[30] W. Hussain, M. T. Sadiq, S. Siuly, and A. U. Rehman, "Epileptic seizure detection using 1 D-convolutional long short-term memory neural networks," *Appl. Acoust.*, vol. 177, Jun. 2021, Art. no. 107941.

[31] F. Es haghi, J. Frounchi, P. Shahabi, and M. Sadighi, "Absence epilepsy seizure onsets detection based on ECG signal analysis," presented at the 20th Iranian Conf. Biomed. Eng. (ICBME), Dec. 2013, pp. 219–222.

[32] G. Shamim, Y. U. Khan, M. Sarfraz, and O. Farooq, "Epileptic seizure detection using heart rate variability," in *Proc. Int. Conf. Signal Process. Commun. (ICSC)*, Dec. 2016.

[33] T. De Cooman *et al.*, "Adaptive nocturnal seizure detection using heart rate and low-complexity novelty detection," *Seizure*, vol. 59, pp. 48–53, Jul. 2018.

[34] S. Nasehi and H. Pourghassem, "Real-time seizure detection based on EEG and ECG fused features using Gabor functions," presented at the Int. Conf. Intell. Comput. Bio-Med. Instrum., Wuhan, China, 2011.

[35] S. Supriya, S. Siuly, H. Wang, and Y. Zhang, "New feature extraction for automated detection of epileptic seizure using complex network framework," *Appl. Acoust.*, vol. 180, Sep. 2021, Art. no. 108098.

[36] R. G. Andrzejak, K. Lehnertz, F. Mormann, C. Rieke, P. David, and C. E. Elger, "Indications of nonlinear deterministic and finite-dimensional structures in time series of brain electrical activity: Dependence on recording region and brain state," *Phys. Rev. E, Stat. Phys. Plasmas Fluids Relat. Interdiscip. Top.*, vol. 64, no. 6, Nov. 2001, Art. no. 061907.

[37] A. Shoeb, "Application of machine learning to epileptic seizure onset detection and treatment," Ph.D. dissertation, Massachusetts Inst. Technol., Cambridge, MA, USA, 2009.

[38] *The Freiburg EEG database*. Accessed: Oct. 10, 2021. [Online]. Available: http://epilepsy.uni-freiburg.de/freiburg-seizure-predictionproject/eeg-database.

[39] M. Ihle *et al.*, "EPILEPSIAE—A European epilepsy database," *Comput. Methods Programs Biomed.*, vol. 106, pp. 127–138, Jun. 2012.

[40] K. Fujiwara *et al.*, "Epileptic seizure prediction based on multivariate statistical process control of heart rate variability features," *IEEE Trans. Biomed. Eng.*, vol. 63, no. 6, pp. 1321–1332, Jun. 2016.

[41] N. Sabor, Y. Li, Z. Zhang, Y. Pu, G. Wang, and Y. Lian, "Detection of the interictal epileptic discharges based on wavelet bispectrum interaction and recurrent neural network," *Sci. China Inf. Sci.*, vol. 64, no. 6, pp. 1–19, Jun. 2021.

[42] F. Mormann, T. Kreuz, R. G. Andrzejak, P. David, K. Lehnertz, and C. E. Elger, "Epileptic seizures are preceded by a decrease in synchronization," *Epilepsy Res.*, vol. 53, pp. 85–173, Mar. 2003.

[43] I. Obeid and J. Picone, "The temple university hospital EEG data corpus," *Frontiers Neurosci.*, vol. 10, pp. 1–5, May 2016.

[44] (Nov. 16, 2021). *The TUH EEG Seizure Corpus (TUSZ)*. [Online]. Available: https://isip.piconepress.com/projects/tuh_eeg/html/downloads.shtml

[45] C. E. Stafstrom and L. Carmant, "Seizures and epilepsy: An overview for neuroscientists," *Cold Spring Harbor Perspect. Med.*, vol. 5, pp. 1–18, Jun. 2015.

[46] S. Roy, I. Kiral-Kornek, and S. Harrer, "ChronoNet: A deep recurrent neural network for abnormal EEG identification," presented at the Artif. Intell. Med. AIME, in Lecture Notes in Computer Science. Cham, Switzerland: Springer, Jan. 2019.

[47] S. M. Usman, M. Usman, and S. Fong, "Epileptic seizures prediction using machine learning methods," *Comput. Math. Methods Med.*, vol. 2017, pp. 1–11, Dec. 2017.

[48] A. Bhattacharyya, L. Singh, and R. B. Pachori, "Fourier–Bessel series expansion based empirical wavelet transform for analysis of non-stationary signals," *Digit. Signal Process.*, vol. 78, pp. 185–196, Jul. 2018.

[49] M. Nazari and S. M. Sakhaei, "Successive variational mode decomposition," *Signal Process.*, vol. 174, Sep. 2020, Art. no. 107610.

[50] A. Cicone, "Iterative filtering as a direct method for the decomposition of nonstationary signals," *Numer. Algorithms*, vol. 85, no. 3, pp. 811–827, Nov. 2020.

[51] Q. Zhang, Q. Xie, K. Duan, B. Liang, M. Wang, and G. Wang, "A digital signal processor (DSP)-based system for embedded continuous-time cuffless blood pressure monitoring using single-channel PPG signal," *Sci. China Inf. Sci.*, vol. 63, no. 4, pp. 1–3, Mar. 2020.

[52] P. A. Muñoz-Gutiérrez, E. Giraldo, M. Bueno-López, and M. Molinas, "Localization of active brain sources from EEG signals using empirical mode decomposition: A comparative study," *Frontiers Integrative Neurosci.*, vol. 12, pp. 1–14, Nov. 2018.

[53] J. Pan and W. J. Tompkins, "A real-time QRS detection algorithm," *IEEE Trans. Biomed. Eng.*, vol. BE-32, no. 3, pp. 230–236, Mar. 1985.

[54] D. Kumar, R. Jadeja, and S. Pande, "Wavelet bispectrum-based nonlinear features for cardiac murmur identification," *Cogent Eng.*, vol. 5, pp. 1–12, Jul. 2018.

[55] M. A. K. Elsayed, "Wavelet bicoherence analysis of wind-wave interaction," *Ocean Eng.*, vol. 33, pp. 458–470, Mar. 2006.

[56] E. Bou Assi, L. Gagliano, S. Rihana, D. K. Nguyen, and M. Sawan, "Bispectrum features and multilayer perceptron classifier to enhance seizure prediction," *Sci. Rep.*, vol. 8, no. 1, pp. 1–8, Oct. 2018.

[57] C. Hou, H. Han, Z. Liu, and M. Su, "A wind direction forecasting method based on Z_score normalization and long short_ term memory," in *Proc. IEEE 3rd Int. Conf. Green Energy Appl. (ICGEA)*, Mar. 2019, pp. 172–176.

[58] H. Peng, F. Long, and C. Ding, "Feature selection based on mutual information criteria of max-dependency, max-relevance, and min-redundancy," *IEEE Trans. Pattern Anal. Mach. Intell.*, vol. 27, no. 8, pp. 1226–1238, Aug. 2005.

[59] C. Nwankpa, W. Ijomah, A. Gachagan, and S. Marshall, "Activation functions: Comparison of trends in practice and research for deep learning," presented at the 2nd Int. Conf. Comput. Sci. Technol., Jamshoro, Pakistan, 2020.

[60] S. B. Wilson, M. L. Scheuer, C. Plummer, B. Young, and S. Pacia, "Seizure detection: Correlation of human experts," *Clin. Neurophysiol.*, vol. 114, no. 11, pp. 2156–2164, Nov. 2003.

[61] A. Estabrooks, T. Jo, and N. Japkowicz, "A multiple resampling method for learning from imbalanced data sets," *Comput. Intell.*, vol. 20, no. 1, pp. 18–36, Feb. 2004.